Proceedings of the International Workshop "Oxide Materials for Electronic Engineering" (OMEE-2009), Lviv 2009

Symmetry Pattern and Domain Wall Structure in $GdFeO_3$ Perovskite Type

D. Savytskii[a,b], T. Tataryn[a] and U. Bismayer[c]

[a]Lviv Polytechnic National University, 12 Bandera St., 79013 Lviv, Ukraine

[b]SRC "Carat", 202 Stryjska St., 79031 Lviv, Ukraine

[c]Universität Hamburg, Grindelallee 48, D-20146 Hamburg, Germany

Symmetry relations between the domain states in $GdFeO_3$ type crystals have been obtained using group-theoretical analysis for prototype and ferroelastic space groups. Models for possible domain pairs are developed. The ion locations on the domain boundary were estimated as intermediate positions between the sites in crystal structure of neighboring domain states. It is shown that the crystalline structure of the boundary approaches to the prototype phase structure — the ideal ABO_3 perovskite-type structure, however certain deformations remain. In addition to the shifts of the all ions the tilts of oxygen octahedra of the some type and related displacements of A ions should take place during the switching of orientation states. The tilts of octahedra and displacements of A ions are sufficient to form translation states (antiphase domains). Antiphase domains can have boundaries between themselves basically along the three faces of the orthorhombic cell.

PACS numbers: 61.72.Mm, 61.72.−y, 61.50.Ah

1. Introduction

The perovskite-type structure is adopted by a large number of oxide compounds with stoichiometry ABO_3. The ideal perovskite structure is characterized by a cubic framework of corner-linked BO_6 octahedra, with large A cations occupying dodecahedral cavities in 12-fold coordination. The corresponding space group of cubic symmetry is $Pm\bar{3}m$, and the unit cell contains one formula unit ($Z = 1$). Under ambient conditions many perovskite-type materials turn out to be distorted from the ideal cubic structural arrangement. A large number of phases occur due to atomic displacements from their high symmetry cubic positions. Among those low symmetry (distorted) perovskites many phases exhibit ferroelastic behavior where the cubic structure is the prototype modification (parent phase).

One of the most prominent phase among the ABO_3 compounds is the orthorhombically distorted perovskite structure of the $GdFeO_3$ type (space group $Pbnm$, $Z = 4$). The distortion is characterized by $a^-a^-c^+$ type tilts of BO_6 octahedra using Glazer's notation [1], with the octahedra themselves remaining essentially undistorted. The B cations remain located at the geometrical centers of the octahedra. However, the A cations are displaced from the centers of the dodecahedral sites, decreasing their coordination to 8 (Fig. 1). This distortion is commonly encountered in perovskite-type materials, for example in: rare-earth aluminates [2–4], $YAlO_3$ [5], gallates [6–8], ferrites [9–11], titanates [12, 13] under normal conditions and in some silicates at high pressures [14], causing ferroelastic properties as well as the appearance of antiphase boundaries [15, 16]. The behavior of domains can strongly influence materials qualities, for example, the configuration of the magnetic domain structure in the solid state solution of rare-earth manganites [17]. Interactions of point defects with domain boundaries determine a whole series of physical properties in such materials with perovskite-type structure, recently used for different technical applications. Among them there is a large group of compounds, having unique dielectric, ferroelectric properties [18–21], as well as ionic [22, 23] and high-temperature electronic conductivity [24].

Ferroic domain structures have been investigated in a large number of chemical compositions with the structure of the $GdFeO_3$ type: natural and synthetic $CaTiO_3$ crystals [12, 25–28], $(Mg,Fe)SiO_3$ [14, 26], $CaGeO_3$, $MnGeO_3$, $SmAlO_3$ [14], $LaGaO_3$ [29–34], $NdGaO_3$ [8, 35]. Experimental techniques were optical microscopy [8, 25, 31, 33, 35], X-ray diffraction [8, 25, 30, 33, 35], high-resolution electron microscopy and selected-area electron diffraction [14, 26–28]. X-ray topography [29, 32, 34] allowed to find the orientation of domain states or the composition planes between domains. Various models of domain pairs have been developed to explain the experimental results.

There are still some ambiguities in the understanding of the domain structure because perovskite-type crystals of the $GdFeO_3$ have a relatively complicated crystal structure. Hence, possible and plausible symmetry operations have to be selected. The aim of this study is to

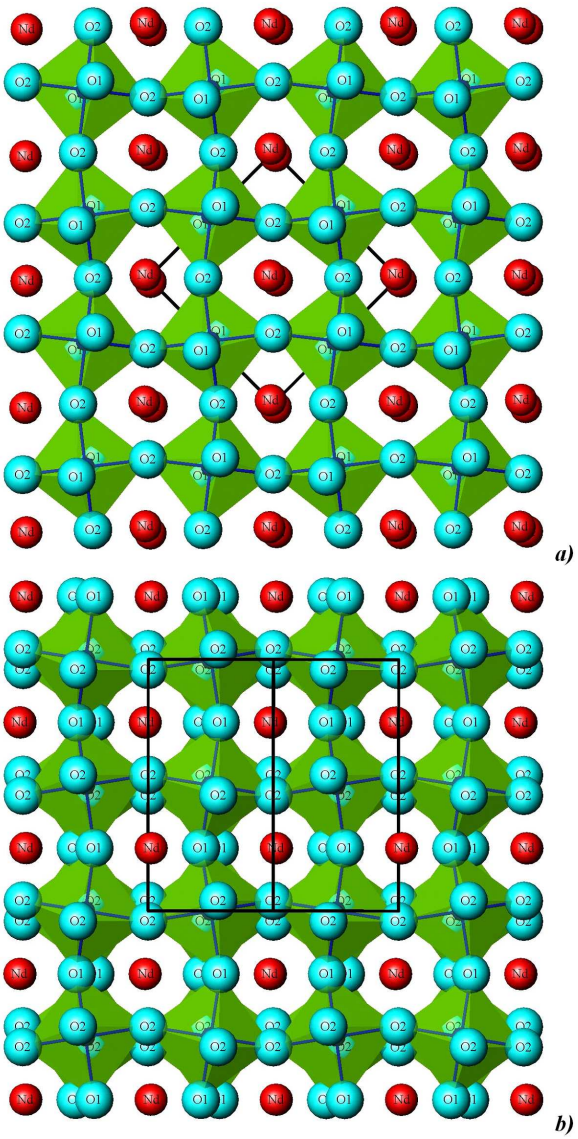

Fig. 1. The perovskite-type structure of $GdFeO_3$ projected along $\langle 001\rangle_p$ (a) and $\langle 100\rangle_p$ (b). Lines mark the orthorhombic unit cell.

determine the symmetry operations, which relate different domain states in compounds of the $GdFeO_3$-type, as well as to improve the crystallographic understanding of the domain walls on the atomic scale.

2. Group-theoretical analysis of space groups

In a previous paper [35] the decomposition of the point group $G = \{m\bar{3}m\}$ of the cubic perovskite parent phase into left cosets with respect to $F = \{mmm\}$ (point group of the ferroelastic distorted phase) was used for group-theoretical analysis [36] of the domain structure of $NdGaO_3$. This approach permitted to determine the number of orientation states in $NdGaO_3$ type crystals ($q = 6$) and the symmetry operations which relate those states geometrically. The material crystallizes in the $GdFeO_3$-type structure which can be considered as a stretched perovskite cubic cell along the face diagonal [110]. Stretching along the other five equivalent face diagonals of the cube enables equivalent distortions of the cell, but differently oriented in space. Hence, there occur 6 possible orientation states (domains) in the ferroelastic distorted phase.

The cell under consideration contains 4 formulae per unit. Hence, the cell volume is 4 times larger than that of the ideal cubic perovskite cell. This means that in addition to the loss of point group symmetry elements in the low symmetry phase a loss of translational operations takes place. Therefore, 4 domains due to translation states (antiphase domains) [37] occur. Six orientation states can be separated and $k = 4$ translational ones. This leads to $q \times k = 24$ symmetry allowed states in the $GdFeO_3$-type crystals. The domains are related by symmetry operations Q_i of the $Pm\bar{3}m$ space group, which are absent in the ferroelastic phase $Pbnm$.

Symmetry operations, which connect state T_1 with the other 23 possible states, are determined by the decomposition of the $Pm\bar{3}m$ symmetry group into 24 left cosets of the $Pbnm$ group of the ferroelastic phase according to

$$\{Pm\bar{3}m\} = \sum_{i=1}^{24} Q_i \times \{Pbnm\}\,. \tag{1}$$

The symmetry operations of the space groups $Pbnm$ and $Pm\bar{3}m$ are taken using the International Tables for Crystallography [38].

The symbols $h_i(\boldsymbol{t}_i)$ are used to designate the space group symmetry elements Q_i. The elements Q_i are a combination of the element h_i of the point group localized in a fixed point of the lattice (origin O) and the translation $\boldsymbol{t}_i$. Space group symmetry element Q_k, which is localized in another point of lattice, can be moved to origin O. Then such space group symmetry element Q_k can be presented as a combination of the element h_k of the point group just localized in the origin O and the "new" translation $\boldsymbol{t}'_k$, which is the sum of the translation $\boldsymbol{t}_k$ and the translation $(-2\boldsymbol{\tau}_i)$, where $\boldsymbol{\tau}_i$ is the vector displacement from the old position of the symmetry element Q_k to the origin O.

The position of the B atom with coordinates $(\frac{1}{2}\ 0\ 0)$ (orthorhombic cell) [8] is chosen as the origin O (Fig. 2). Then the space group $Pbnm$ (or $Pnma$ according to international standard) has the following space group symmetry elements: identity *1*; inversion centre $\bar{1}(0,0,0)$ localized in origin O; mirror plane m_{001} placed at $z = 1/4$; "diagonal" glide plane $n_{010}(\frac{1}{2},0,\frac{1}{2})$ placed at $y = 1/4$; glide plane $b_{100}(0,\frac{1}{2},0)$ placed at $x = 1/4$; twofold screw axis $2_{001}(0,0,\frac{1}{2})$, which passes through origin O; twofold screw axes $2_{010}(0,\frac{1}{2},0)$ and $2_{100}(\frac{1}{2},0,0)$, which are localized at $x = 1/4$, $z = 1/4$ and $y = 1/4$, $z = 0$ (Fig. 2a), correspondingly. Other symmetry operations of the cell are excluded from our considerations because their operation can be presented as a combination of operations mentioned above and translations $\boldsymbol{a}$, $\boldsymbol{b}$, $\boldsymbol{c}$ (orthorhombic cell parameters), or their lin-

ear combinations. Adding the corresponding translation $(-2\boldsymbol{\tau}_i)$, we can localize the planes and the axes in origin O (Fig. 2b). Then the space group symmetry elements of the space group $Pbnm$ can be presented as identity $1(0,0,0)$; inversion centre $\bar{1}(0,0,0)$; mirror planes $m_{001}(0,0,\frac{1}{2})$; $m_{010}(\frac{1}{2},\frac{1}{2},\frac{1}{2})$; $m_{100}(\frac{1}{2},\frac{1}{2},0)$; twofold axes $2_{001}(0,0,\frac{1}{2})$; $2_{010}(\frac{1}{2},\frac{1}{2},\frac{1}{2})$; $2_{100}(\frac{1}{2},\frac{1}{2},0)$. We rewrite these elements using the coordinate system of the perovskite cell: $1(0,0,0)$, $\bar{1}(0,0,0)$, $m_z(0,0,1)$, $2_z(0,0,1)$, $m_{xy}(1,0,1)$, $2_{xy}(1,0,1)$, $m_{-xy}(1,0,0)$ and $2_{-xy}(1,0,0)$ considering the perovskite cell as $\frac{1}{2}\boldsymbol{c}=\boldsymbol{c}_{\rm p}$, $\frac{1}{2}\boldsymbol{b}-\frac{1}{2}\boldsymbol{a}=\boldsymbol{b}_{\rm p}$ and $\frac{1}{2}\boldsymbol{b}+\frac{1}{2}\boldsymbol{a}=\boldsymbol{a}_{\rm p}$ (Fig. 2b). It is significant that the elements of space group $Pbnm$ are a combination of the elements of the point group mmm localized in origin O and three perovskites translations $(0,0,1)$, $(1,0,0)$ and $(1,0,1)$.

TABLE

Decomposition of $Pm\bar{3}m$ into left cosets of $Pbnm$ and appropriate domains. OST — orientation state.

OST	Situation	Symmetry operations of space group $Pm\bar{3}m$							
D_1	T_1	$1(0,0,0)$	$\bar{1}(0,0,0)$	$m_z(0,0,1)$	$2_z(0,0,1)$	$m_{xy}(1,0,1)$	$2_{xy}(1,0,1)$	$m_{-xy}(1,0,0)$	$2_{-xy}(1,0,0)$
	T_2	$1(0,0,1)$	$\bar{1}(0,0,1)$	$m_z(0,0,0)$	$2_z(0,0,0)$	$m_{xy}(1,0,0)$	$2_{xy}(1,0,0)$	$m_{-xy}(1,0,1)$	$2_{-xy}(1,0,1)$
	T_3	$1(1,0,1)$	$\bar{1}(1,0,1)$	$m_z(1,0,0)$	$2_z(1,0,0)$	$m_{xy}(0,0,0)$	$2_{xy}(0,0,0)$	$m_{-xy}(0,0,1)$	$2_{-xy}(0,0,1)$
	T_4	$1(1,0,0)$	$\bar{1}(1,0,0)$	$m_z(1,0,1)$	$2_z(1,0,1)$	$m_{xy}(0,0,1)$	$2_{xy}(0,0,1)$	$m_{-xy}(0,0,0)$	$2_{-xy}(0,0,0)$
D_2	T_5	$m_x(0,0,0)$	$2_x(0,0,0)$	$2_y(0,0,1)$	$m_y(0,0,1)$	$4_z^3(1,0,1)$	$\bar{4}_z^3(1,0,1)$	$4_z(1,0,0)$	$\bar{4}_z(1,0,0)$
	T_6	$m_x(0,0,1)$	$2_x(0,0,1)$	$2_y(0,0,0)$	$m_y(0,0,0)$	$4_z^3(1,0,0)$	$\bar{4}_z^3(1,0,0)$	$4_z(1,0,1)$	$\bar{4}_z(1,0,1)$
	T_7	$m_x(1,0,1)$	$2_x(1,0,1)$	$2_y(1,0,0)$	$m_y(1,0,0)$	$4_z^3(0,0,0)$	$\bar{4}_z^3(0,0,0)$	$4_z(0,0,1)$	$\bar{4}_z(0,0,1)$
	T_8	$m_x(1,0,0)$	$2_x(1,0,0)$	$2_y(1,0,1)$	$m_y(1,0,1)$	$4_z^3(0,0,1)$	$\bar{4}_z^3(0,0,1)$	$4_z(0,0,0)$	$\bar{4}_z(0,0,0)$
D_3	T_9	$m_{xz}(0,0,0)$	$2_{xz}(0,0,0)$	$4_y(1,0,0)$	$\bar{4}_y(1,0,0)$	$3_{x-y-z}(1,0,1)$	$\bar{3}_{x-y-z}(1,0,1)$	$3_{-x-yz}(0,0,1)$	$\bar{3}_{-x-yz}(0,0,1)$
	T_{10}	$m_{xz}(0,0,1)$	$2_{xz}(0,0,1)$	$4_y(1,0,1)$	$\bar{4}_y(1,0,1)$	$3_{x-y-z}(1,0,0)$	$\bar{3}_{x-y-z}(1,0,0)$	$3_{-x-yz}(0,0,0)$	$\bar{3}_{-x-yz}(0,0,0)$
	T_{11}	$m_{xz}(1,0,1)$	$2_{xz}(1,0,1)$	$4_y(0,0,1)$	$\bar{4}_y(0,0,1)$	$3_{x-y-z}(0,0,0)$	$\bar{3}_{x-y-z}(0,0,0)$	$3_{-x-yz}(1,0,0)$	$\bar{3}_{-x-yz}(1,0,0)$
	T_{12}	$m_{xz}(1,0,0)$	$2_{xz}(1,0,0)$	$4_y(0,0,0)$	$\bar{4}_y(0,0,0)$	$3_{x-y-z}(0,0,1)$	$\bar{3}_{x-y-z}(0,0,1)$	$3_{-x-yz}(1,0,1)$	$\bar{3}_{-x-yz}(1,0,1)$
D_4	T_{13}	$m_{-xz}(0,0,0)$	$2_{-xz}(0,0,0)$	$4_y^3(1,0,0)$	$\bar{4}_y^3(1,0,0)$	$3_{-xy-z}(1,0,1)$	$\bar{3}_{-xy-z}(1,0,1)$	$3_{xyz}(0,0,1)$	$\bar{3}_{xyz}(0,0,1)$
	T_{14}	$m_{-xz}(0,0,1)$	$2_{-xz}(0,0,1)$	$4_y^3(1,0,1)$	$\bar{4}_y^3(1,0,1)$	$3_{-xy-z}(1,0,0)$	$\bar{3}_{-xy-z}(1,0,0)$	$3_{xyz}(0,0,0)$	$\bar{3}_{xyz}(0,0,0)$
	T_{15}	$m_{-xz}(1,0,1)$	$2_{-xz}(1,0,1)$	$4_y^3(0,0,1)$	$\bar{4}_y^3(0,0,1)$	$3_{-xy-z}(0,0,0)$	$\bar{3}_{-xy-z}(0,0,0)$	$3_{xyz}(1,0,0)$	$\bar{3}_{xyz}(1,0,0)$
	T_{16}	$m_{-xz}(1,0,0)$	$2_{-xz}(1,0,0)$	$4_y^3(0,0,0)$	$\bar{4}_y^3(0,0,0)$	$3_{-xy-z}(0,0,1)$	$\bar{3}_{-xy-z}(0,0,1)$	$3_{xyz}(1,0,1)$	$\bar{3}_{xyz}(1,0,1)$
D_5	T_{17}	$m_{yz}(0,0,0)$	$2_{yz}(0,0,0)$	$4_x^3(1,0,0)$	$\bar{4}_x^3(1,0,0)$	$3^2_{-xy-z}(0,0,0)$	$\bar{3}^2_{-xy-z}(0,0,0)$	$3^2_{-x-yz}(1,0,0)$	$\bar{3}^2_{-x-yz}(1,0,0)$
	T_{18}	$m_{yz}(0,0,1)$	$2_{yz}(0,0,1)$	$4_x^3(1,0,1)$	$\bar{4}_x^3(1,0,1)$	$3^2_{-xy-z}(0,0,1)$	$\bar{3}^2_{-xy-z}(0,0,1)$	$3^2_{-x-yz}(1,0,1)$	$\bar{3}^2_{-x-yz}(1,0,1)$
	T_{19}	$m_{yz}(1,0,1)$	$2_{yz}(1,0,1)$	$4_x^3(0,0,1)$	$\bar{4}_x^3(0,0,1)$	$3^2_{-xy-z}(1,0,1)$	$\bar{3}^2_{-xy-z}(1,0,1)$	$3^2_{-x-yz}(0,0,1)$	$\bar{3}^2_{-x-yz}(0,0,1)$
	T_{20}	$m_{yz}(1,0,0)$	$2_{yz}(1,0,0)$	$4_x^3(0,0,0)$	$\bar{4}_x^3(0,0,0)$	$3^2_{-xy-z}(1,0,0)$	$\bar{3}^2_{-xy-z}(1,0,0)$	$3^2_{-x-yz}(0,0,0)$	$\bar{3}^2_{-x-yz}(0,0,0)$
D_6	T_{21}	$m_{-yz}(0,0,0)$	$2_{-yz}(0,0,0)$	$4_x(1,0,0)$	$\bar{4}_x(1,0,0)$	$3^2_{x-y-z}(0,0,0)$	$\bar{3}^2_{x-y-z}(0,0,0)$	$3^2_{xyz}(1,0,0)$	$\bar{3}^2_{xyz}(1,0,0)$
	T_{22}	$m_{-yz}(0,0,1)$	$2_{-yz}(0,0,1)$	$4_x(1,0,1)$	$\bar{4}_x(1,0,1)$	$3^2_{x-y-z}(0,0,1)$	$\bar{3}^2_{x-y-z}(0,0,1)$	$3^2_{xyz}(1,0,1)$	$\bar{3}^2_{xyz}(1,0,1)$
	T_{23}	$m_{-yz}(1,0,1)$	$2_{-yz}(1,0,1)$	$4_x(0,0,1)$	$\bar{4}_x(0,0,1)$	$3^2_{x-y-z}(1,0,1)$	$\bar{3}^2_{x-y-z}(1,0,1)$	$3^2_{xyz}(0,0,1)$	$\bar{3}^2_{xyz}(0,0,1)$
	T_{24}	$m_{-yz}(1,0,0)$	$2_{-yz}(1,0,0)$	$4_x(0,0,0)$	$\bar{4}_x(0,0,0)$	$3^2_{x-y-z}(1,0,0)$	$\bar{3}^2_{x-y-z}(1,0,0)$	$3^2_{xyz}(0,0,0)$	$\bar{3}^2_{xyz}(0,0,0)$

For the space group $Pm\bar{3}m$ the symmetry elements localized at the origin (B atom) are 48 space group symmetry elements $h_i(0,0,0)$, where h_i is a symmetry element of the point group $m\bar{3}m$ [38]. Symmetry elements of the types $h_i(0,0,1)$, $h_i(1,0,0)$ and $h_i(1,0,1)$ are also peculiar to the $Pm\bar{3}m$ group. This means that in addition to the reduction of point group symmetry from $m\bar{3}m$ to mmm in the low symmetry phase a loss of translational operations $(0,0,1)$, $(1,0,0)$ and $(1,0,1)$ takes place.

In a result, symmetry elements of the types $h_i(0,0,1)$, $h_i(1,0,0)$ and $h_i(1,0,1)$ should be added in the set of the $Pm\bar{3}m$ group and the total number of elements increase to $48\times 4=192$. Symmetry operations, which connect state T_1 with the other 23 possible states are determined by the decomposition of these 192 elements of $Pm\bar{3}m$ symmetry group into 24 left cosets of the $Pbnm$ group (8 space group symmetry elements) of the ferroelastic phase.

In a first step the following operations $1(0,0,0)$, $1(0,0,1)$, $1(1,0,1)$ and $1(1,0,0)$ (the three last operations are translations inherent in $Pm\bar{3}m$) were applied as Q_i. The symmetry elements of the corresponding left cosets are presented in the first four rows of Table. The first left coset includes symmetry operations of the space group $Pbnm$ which leave the state T_1 invariant. Three other left cosets are combinations of elements of the point group mmm (1, 2_z, 2_{xy}, 2_{-xy}, $\bar{1}$, m_z, m_{xy}, m_{-xy}) and the above mentioned perovskite cell translations. These symmetry operations leave the system of crystallographic axis unchanged and therefore, the obtained left cosets obtained are a set of operations, which transform the state T_1 into T_2, T_3 or T_4 (antiphase domains). Such regions can have boundaries along 3 perpendicular planes $(001)_{\rm p}$, $(110)_{\rm p}$ and $(\bar{1}10)_{\rm p}$, which are included in the corresponding left coset and which are parallel to the faces of the orthorhombic cell.

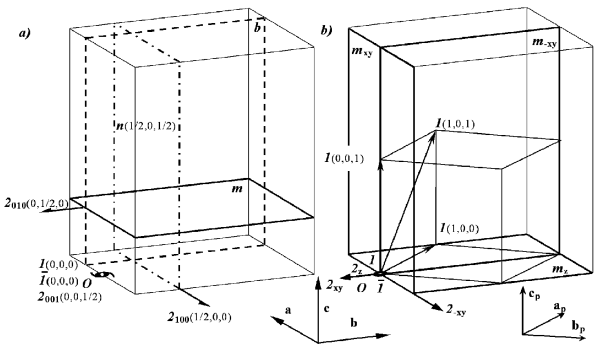

Fig. 2. Relationship between unit cells of prototype and ferrophase for $GdFeO_3$ crystals and localization of the symmetry elements of the space group $Pbnm$ before (a) and after (b) moving to origin O.

The element $m_x(0,0,0)$ and its combinations with translations $(0,0,1)$, $(1,0,1)$ and $(1,0,0)$ were selected as the next four generating elements Q_i. The elements of the point group $m\bar{3}m$, which are absent in the point group mmm and which are the operations relating the orientation states D_1 and D_2 (see Table 1 in [35]) with each other, are included in the corresponding left cosets. The elements of the left cosets for T_6, T_7 and T_8 can be obtained by acting step by step on the left coset for T_5 using the translations $(0,0,1)$, $(1,0,1)$ and $(1,0,0)$. This procedure demonstrates that the orientation state D_2 can be split into four antiphase domains.

The corresponding left cosets for the other T_9–T_{24} states of the D_3–D_6 orientation domains were obtained by selecting the corresponding mirror planes $m_{xz}(0,0,0)$, $m_{-xz}(0,0,0)$, $m_{yz}(0,0,0)$ and $m_{-yz}(0,0,0)$ and their combinations with translations $(0,0,1)$, $(1,0,1)$ and $(1,0,0)$ as Q_i (Table).

3. Crystalline structure of domain walls

Using symmetry operations to relate the different states T_1–T_i (Table) and the schematic representation of the studied perovskite-type structure on the basis of Glazer's classification of octahedral rotations we construct configurations of the corresponding pairs of states in neodymium gallate $NdGaO_3$. It was selected as an example to demonstrate the crystalline structure of domain walls. For schematic representation of the structure of the materials investigated we used a modified Glazer scheme. We added the displacement of A ions and the magnitudes for octahedral tilts to schematic diagrams proposed by Glazer [1]. The magnitudes of the tilts for each octahedron are indicated symbolically by a set of three letters, which refer to the perovskite axes. Each set of three letters refers to one octahedron. Repeating the appropriate letter denotes equality of the corresponding magnitudes. Similar to Glazer's scheme we used superscripts + or – to show defined positive or negative tilt about the corresponding pseudocubic axis. The displacement of A-cations from center of dodecahedral anion environment is indicated by line and fill circle in gaps of octahedral framework. The fragment of the crystal structure and the corresponding scheme for the T_1 state are shown in Figs. 1 and 3. This technique can be applied to other crystals of $GdFeO_3$ type structure with similar distortions of the ideal perovskite structure but with different magnitudes of anion octahedral tilts and other displacements of the rare-earth ions.

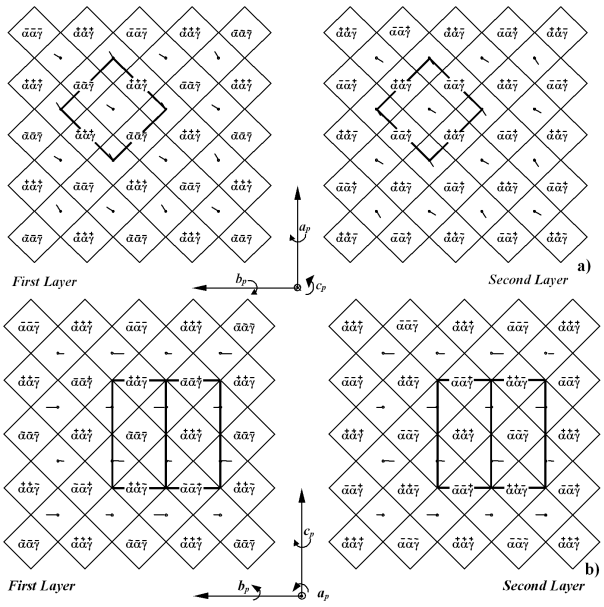

Fig. 3. Schematic representation of the $NdGaO_3$ structure projection on $(001)_p$ (a) and $(100)_p$ (b) planes. Lines mark the orthorhombic unit cell.

We may assume here that the boundary width between a pair of domain states corresponds to only one layer of oxygen octahedra (one perovskite cell parameter) and such boundary is not necessarily the high symmetry cubic modification. The twin boundary (boundary between orientation states) in crystals may extend to a few cell parameters [39].

The ionic positions of T_2, T_3 and T_4 were obtained by applying the operation $m_{xy}(1,0,0)$ for T_2; $m_{xy}(0,0,0)$ — for T_3; $m_{xy}(0,0,1)$ — for T_4 to the ions of the T_1 state. The ionic arrangement on the interface between T_1 and T_i were estimated as the intermediate between the positions given by the periodic crystal structure of T_1 and T_i. The structure of the states T_1–T_2, T_1–T_3 and T_1–T_4 are shown in Fig. 4. Here the boundary in orthorhombic coordinates is parallel to the (010) plane. As shown in Fig. 4, the interface approaches the structure of the prototype phase — the ideal perovskite arrangement, though certain distortions remain. The distortion of the structure on the boundary depends on the states, which are separated by the interface. The tilts of oxygen octahedra around two perovskite axes take place for the domain pair T_1–T_3. Using Glazer notation [1] this tilt system is described by $a^0b^-b^-$. Such tilts produce

structure belonging to space group $Imma$, if we do not take into account the displacement of A cations at domain boundary. For the domain pair T_1–T_2 octahedrons are rotated around one perovskite axis only and crystal structure can be attributed to tilt system $a^0a^0c^+$ and space group $P4/mbm$. For the domain pair T_1–T_4 rotations of oxygen octahedra are absent $a^0a^0a^0$, i.e. $Pm\bar{3}m$. Both space group $P4/mbm$ and $Imma$ is supergroup for $Pbnm$ and subgroup for $Pm\bar{3}m$ [38].

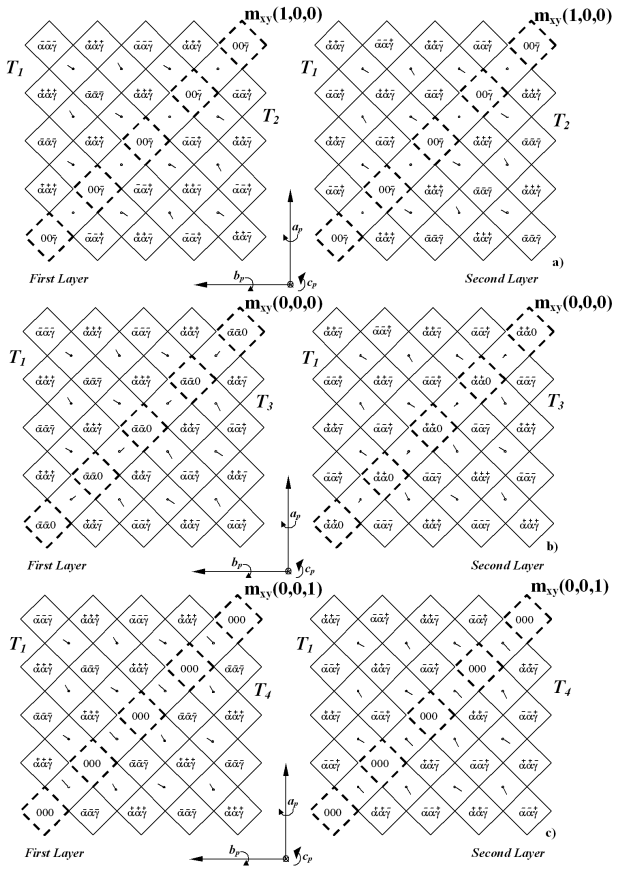

Fig. 4. Schematic representation of the crystal structure on the $(001)_p$ plane for T_1–T_2 (a), T_1–T_3 (b) and T_1–T_4 (c) domain pairs in $NdGaO_3$ crystals.

Three types of antiphase boundaries were observed in $La_{2/3}Ca_{1/3}MnO_3$ (LCMO) due to the loss of translation vectors $\boldsymbol{R}_1 = [0, \frac{1}{2}, 0]$, $\boldsymbol{R}_2 = [\frac{1}{2}, 0, \frac{1}{2}]$, and $\boldsymbol{R}_3 = [\frac{1}{2}, \frac{1}{2}, \frac{1}{2}]$ in $Pnma$ space group setting [40]. In these three types, the density of the antiphase boundaries associated with $\boldsymbol{R}_3$ was the highest in LCMO, which is explained by the relatively small deformation of the interstitial A sites along antiphase boundaries (APBs). In the $Pnma$ setting the translation vector $\boldsymbol{R}_3 = [\frac{1}{2}, \frac{1}{2}, \frac{1}{2}]$ corresponds to the vector of the pseudo-perovskite cell $\boldsymbol{t}_3 = (1, 0, 1)$ whereas $\boldsymbol{R}_1 = [0, \frac{1}{2}, 0] - \boldsymbol{t}_2 = (0, 0, 1)$ and $\boldsymbol{R}_2 = [\frac{1}{2}, 0, \frac{1}{2}]$ corresponds to $\boldsymbol{t}_4 = (1, 0, 0)$. Antiphase boundary associated with $\boldsymbol{R}_3$ describes the interface between the T_1 and T_3 domains. Taking into account that the crystalline structure of this boundary is closer to the crystal structure of $Pbnm$, our simulation of the crystalline structure of antiphase boundaries confirms the results received in [40] with a relatively smaller displacement of the interstitial A sites (in other words — the oxygen octahedra are rotated around two perovskites axes, characteristic for the bulk $Pbnm$ crystal structure) along APBs applying $\boldsymbol{R}_3$. Hence the energy of such antiphase boundaries is the lowest in comparison with other possible APBs that leads to their high density in LCMO.

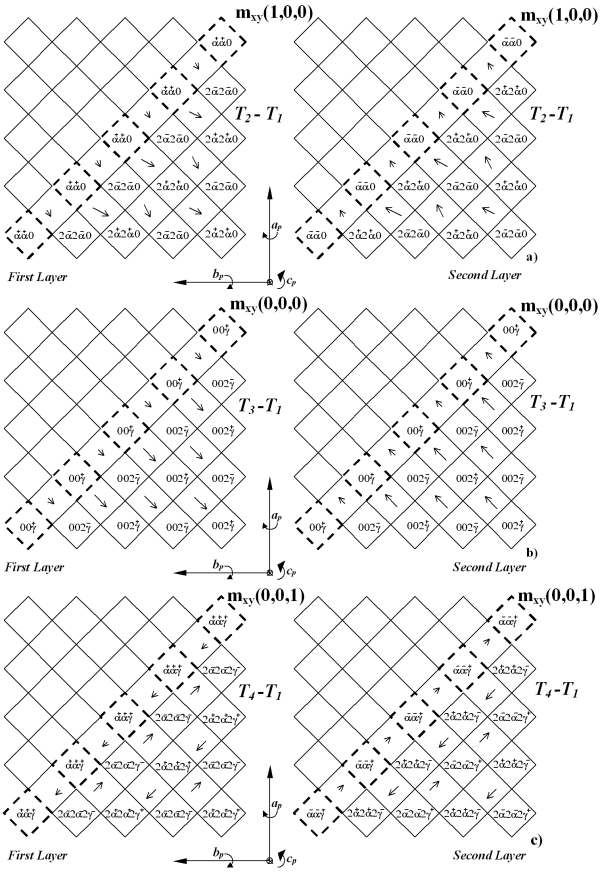

Fig. 5. Ion displacements on switching the T_1 state to T_2 (a), T_3 (b), and T_3 (c) states.

Comparing the ion positions shown in Fig. 1 and Fig. 4 we can determine the displacements in the crystal structure for switching the state T_1 to T_i. For example, for switching state T_1 to T_2 it is necessary that rotations of oxygen octahedra of the $2a^-2a^-0$-type (the Glazer rotations) and displacements of rare-earth ions along $\langle 140 \rangle$ take place. For switching T_1 to T_3 — $002c^+$-type rotations and displacements along $\langle 010 \rangle$; for switching T_1 to T_4 — $2a^-2a^-2c^+$-type rotations and displacements along $\langle 100 \rangle$ are required (Fig. 5). In these cases the Ga ions at the center of oxygen octahedra are not displaced. For T_1 and T_i (i = 2–4) pairs the Ga (B cation) sublattice is generic for both states and leads to merohedral twinning [12]. It is necessary to note that the rotations are twice big as in the deformed $GdFeO_3$ type structures ($Pbnm$).

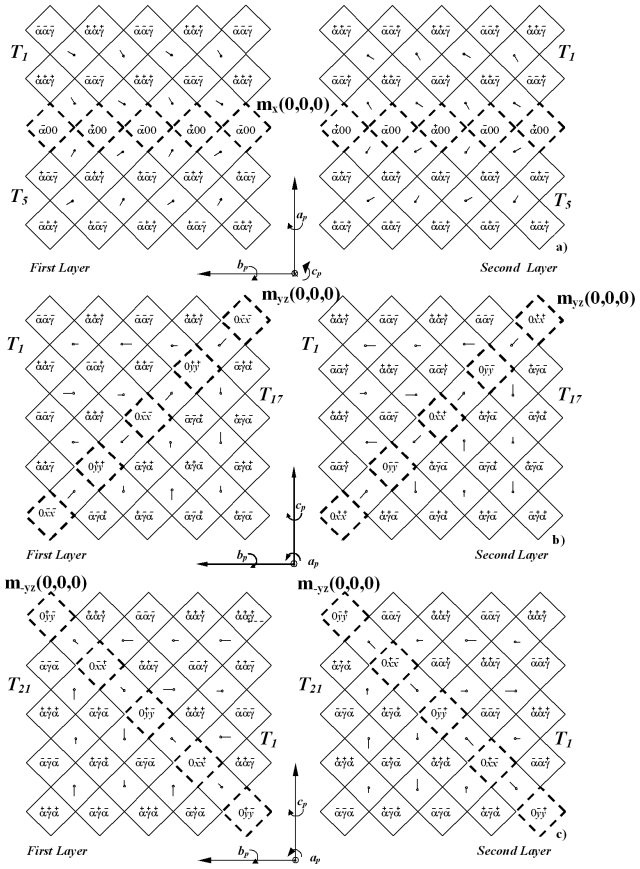

Fig. 6. Schematic representation of the structure on the perovskite planes for T_1–T_5 (a), T_1–T_{17} (b) and T_1–T_{21} (c) domain pairs in $NdGaO_3$; $x = (\frac{1}{2})(\gamma + \alpha)$ and $y = (\frac{1}{2})(\gamma - \alpha)$.

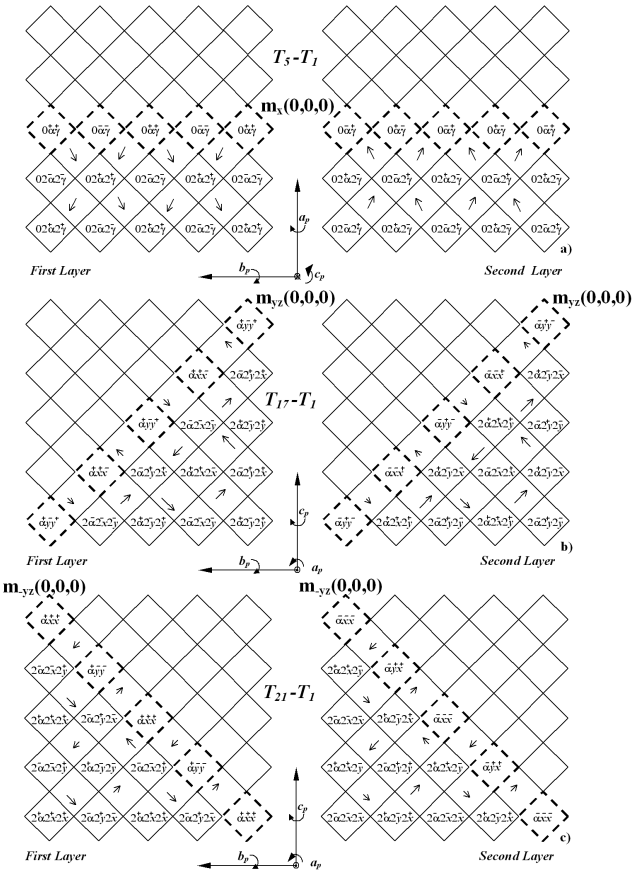

Fig. 7. Ion displacements during the switching of the T_1 state to T_5 (a), T_{17} (b) and T_{21} (c) states with $x = (\frac{1}{2})(\gamma + \alpha)$ nd $y = (\frac{1}{2})(\gamma - \alpha)$.

Similarly the schemes for T_1 and T_i (where i = 5–8) were constructed, considering another D_2 orientation state (Fig. 6a).The boundaries between this pair of orientation states can be parallel to the m_x and m_y perovskite planes. Comparing the scheme shown in Fig. 3 and 6a we can determine the ion displacements necessary to switch the state T_1 to the state T_5 (Fig. 7a). It should be noticed that, in contrast to the T_1–T_2 ... T_1–T_4 pairs which are cases of the same D_1 orientation state, in the T_1–T_5 pair all ions in the structure must see an additional shift along the $[0\bar{1}0]_\mathrm{p}$ direction in the case of the m_x interface (Fig. 8a) [33, 41].

More complicated models are developed for T_1 and T_i situations of the $D_3 \ldots D_6$ orientation states. In Fig. 6b and c the schemes for situations T_1–T_{17} and T_1–T_{21} are given for interfaces parallel to the m_{yz} and m_{-yz} perovskite-type planes, correspondingly. The constructions were made for layers of the crystal structure parallel to the $(100)_\mathrm{p}$ plane, because m_{yz} and m_{-yz} planes are perpendicular. The ion displacements required to switch state T_1 to states T_{17} and T_{21} are illustrated in Fig. 6b, c. During the switching of the state T_1 to the states T_i (i = 2–8) oxygen octahedra rotate with the same phase around c_p and in antiphase — around a_p and b_p by identical angles, whereas for the reorientation of T_1 to T_i (i = 9–24) tilts of different angles occur. In this respect the tilts are synchronised and their orthorhombic cell translation period is kept (Fig. 7b, c).

In addition to the displacements mentioned above, all ions of the structure should be twin shifted along $[\overline{5.76}\,\bar{1}\,1]_\mathrm{p}$ for T_{17} and along $[5.76\,1\,1]_\mathrm{p}$ for T_{21} (Fig. 8b) at room temperature [35, 41].

For the switching of T_1 to T_{17} and T_{21} (separated from T_1 by S-type domain walls) twin shifts in directions $[011]_\mathrm{p}$ and $[01\bar{1}]_\mathrm{p}$ are necessary correspondingly (Fig. 8c) [35, 41]. The rotation by 180° with respect to these directions is a symmetry operation between the corresponding pairs T_1–T_{17} and T_1–T_{21} (Table). Due to their irrational Miller indices, these interfaces cannot be presented in the way which was used for interfaces with rational Miller indices (W-type domain walls). Rotations of oxygen octahedra and displacements of rare-earth ions for such switchings are identical to those of the corresponding pairs T_1–T_i (i = 9–24), separated by W-type domain walls.

The above mentioned is also characteristic for other T_i of orientation states D_5, D_6, D_3 and D_4.

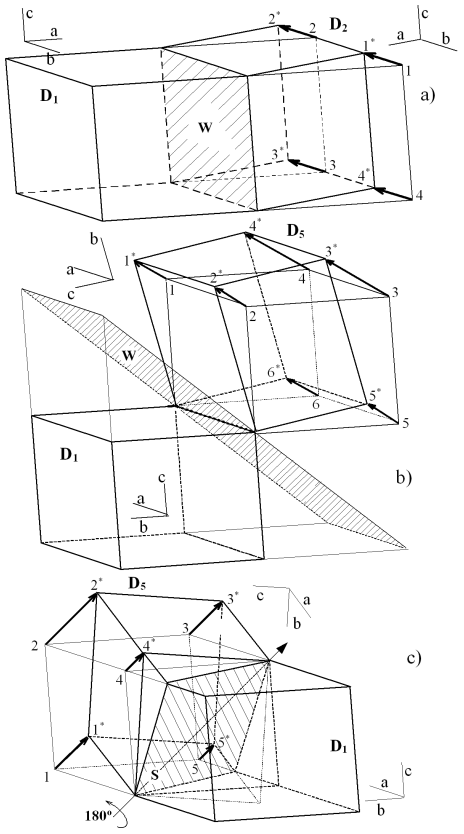

Fig. 8. Shifts in $GdFeO_3$ for the switching of the D_1 orientation state (a) to a D_2 orientation state in a $(100)_p$ domain wall; (b) to D_5 orientation state in a $(0\bar{1}1)_p$ W-type domain wall; (c) to the D_5 orientation state in case of a S-type domain wall.

4. Conclusions

A group-theoretical analysis of prototype $Pm\bar{3}m$ and ferroelastic $Pbnm$ space groups allowed to find the symmetry operations which relate the different domain states in $GdFeO_3$-type crystals. Such domains are geometrically related by symmetry operations of space group $Pm\bar{3}m$, which do not occur in the ferroelastic space group $Pbnm$. Each of the 6 possible orientation states can be separated by 4 translational ones in $GdFeO_3$-type crystals.

The models of the state pairs can be built on the basis of the proposed symmetry operations relating the different domain states. The ion located on the boundary between the states were estimated to be at intermediate positions between the positions in both states. It has been shown that in $GdFeO_3$ type crystals the crystalline structure on the boundary between the domain states always tends towards the prototype phase (the ideal perovskite structure), though certain deformations remain visible.

Ion displacements which occur during switching the states, can be determined by comparing the ion locations in single domain and two domain areas of the crystal. It has been shown that in addition to twin shifts of all ions, tilts of oxygen octahedra of the same type and appropriate displacements of the A ions take place on switching the orientation states in the crystal structure of $GdFeO_3$ type. The tilts of octahedra and displacements of A ions are sufficient to form antiphase domains. Such regions may have boundaries along 3 mutually perpendicular planes $(001)_p$, $(110)_p$ and $(\bar{1}10)_p$, which are parallel to the faces of the orthorhombic cell.

Acknowledgments

The work was supported by WTZ (UKR 07/009) and Ukrainian Ministry of Education and Science (the "Tern" project). T. Tataryn acknowledge financial support of the Deutscher Akademischer Austauschdienst (Leonhard-Euler program).

References

[1] A.M. Glazer, *Acta Crystallogr. B* **28**, 3384 (1972).

[2] S. Geller, V.B. Bala, *Acta Crystallogr.* **9**, 1019 (1956).

[3] A.A. Levin, *Kristallografiya* **37**, 1020 (1992).

[4] M. Marezio, P.D. Dernier, J.P. Remeika, *J. Solid State Chem.* **4**, 11 (1972).

[5] R. Diehl, G. Brandt, *Mater. Res. Bull.* **10**, 85 (1975).

[6] S. Geller, *Acta Crystallogr.* **10**, 243 (1957).

[7] M. Sundberg, P.-E. Werner, M. Westdahl, K. Mazur, *Mater. Sci. Forum* **166-169**, 795 (1994).

[8] S.B. Ubizskii, L.O. Vasylechko, D.I. Savytskii, A.O. Matkovskii, I.M. Syvorotka, *Supercond. Sci. Technol.* **7**, 766 (1994).

[9] P. Coppens, M. Eibschutz, *Acta Crystallogr.* **19**, 524 (1965).

[10] S. Geller, E.A. Wood, *Acta Crystallogr.* **9**, 563 (1956).

[11] M. Marezio, J.P. Remeika, P.D. Dernier, *Acta Crystallogr. B* **26**, 2008 (1970).

[12] A.V. Arakcheeva, D.Ju. Pucharovskii, V.M. Gekimianz, V.A. Popov, G.U. Lubman, *Kristallografiya* **42**, 54 (1997).

[13] D.A. MacLean, H. Ng, J.E. Greedan, *J. Solid State Chem.* **30**, 35 (1979).

[14] Y. Wang, F. Guyot, R.C. Liebermann, *J. Geophys. Res.* **97**, B9, 12327 (1992).

[15] H. Wondratschek, W. Jeitschko, *Acta Crystallogr. A* **32**, 664 (1976).

[16] M. Guymont, *Phys. Rev. B* **18**, 5385 (1978).

[17] G. Jung, V. Markovich, C.J. Beek, D. Mogilyansky, Ya.M. Mukovskii, *Phys. Rev. B* **72**, 134412 (2005).

[18] C. Wang, Q.F. Fang, Y. Shi, Z.G. Zhu, *Mater. Res. Bull.* **36**, 2657 (2001).

[19] H. Frayssignes, M. Gabbay, G. Fantozzi, N.J. Porch, B.L. Cheng, T.W. Button, *J. Eur. Ceram. Soc.* **24**, 2989 (2004).

[20] S.-T. Zhang, G.-L. Yuan, J. Wang, Y.-F. Chen, G.-Xu. Cheng, Z.-G. Liu, *Solid. State Commun.* **132**, 315 (2004).

[21] J.Z. Liu, Y.X. Jia, R.N. Shelton, M.J. Fluss, *Phys. Rev. Lett.* **66**, 1354 (1991).

[22] D. Savytskii, L. Vasylechko, U. Bismayer, C. Paulmann, M. Berkowski, *NATO Science Series* **202**, 135 (2005).

[23] M. Kurumada, E. Iguchi, D. Savytskii, *J. Appl. Phys.* **100**, 014107 (2006).

[24] A.K. Pradhan, Y. Feng, S. Shibata, K. Nakao, N. Koshizuka, *Physica C* **357-360**, 457 (2001).

[25] H.F. Kay, P.C. Bailey, *Acta Crystallogr.* **10**, 219 (1957).

[26] Y. Wang, *Science* **248**, 468 (1990).

[27] Y. Wang, *Science* **251**, 410 (1991).

[28] T.J. White, R.L. Segall, J.C. Barry, J.L. Hutchison, *Acta Crystallogr. B* **41**, 93 (1985).

[29] I.K. Bdikin, I.M. Shmyt'ko, A.M. Balbashov, A.V. Kazansky, *J. Appl. Crystallogr.* **26**, 71 (1993).

[30] G.W. Berkstresser, A.J. Valentino, C.D. Brandle, *J. Cryst. Growth* **109**, 457 (1991).

[31] J. Fink-Finowicki, M. Berkowski, A. Pajaczkowska, *J. Mater. Sci.* **27**, 107 (1992).

[32] A.N. Morozov, O.Ju. Morozova, N.I. Ponomarev, *Kristallografiya* **38**, 149 (1993).

[33] D.I. Savytskii, S.B. Ubizskii, L.O. Vasylechko, A.O. Matkovskii, I.M. Syvorotka, *Functional Materials* (*Kharkiv, Ukraine*) **1**, 55 (1994).

[34] G.-D. Yao, M. Dudley, Y. Wang, X. Liu, R.C. Liebermann, *Mater. Sci. Eng. A* **132**, 23 (1991).

[35] D.I. Savytskii, S.B. Ubizskii, L.O. Vasylechko, I.M. Syvorotka, A.O. Matkovskii, *Acta Phys. Pol. A* **92**, 231 (1997).

[36] V. Janovec, *Czech. J. Phys. B* **22**, 974 (1972).

[37] V.K. Wadhawan, *Phase Transit.* **3**, 3 (1982).

[38] Th. Hahn, *Space-group symmetry*, Vol. A, in: *International Tables for Crystallography*, Kluwer Academic Publ., Dordrecht 2002.

[39] J. Chrosch, E.K.H. Salje, *J. Appl. Phys.* **85**, 722 (1999).

[40] Y. Ding, D.D. Liang, *J. Appl. Phys.* **92**, 5425 (2002).

[41] D.I. Savytskii, S.B. Ubizskii, L.O. Vasylechko, A.O. Matkovskii, *Crystallogr. Rep.* **41**, 859 (1996). [*Kristallografiya (Moscow)* **41**, 902 (1996)].